Journal of Computational Mathematics
Vol.xx, No.x, 2023, 1–17.
http://www.global-sci.org/jcm
doi:10.4208/jcm.2307-m2022-0264

A STABILIZER FREE WEAK GALERKIN FINITE ELEMENT METHOD FOR BRINKMAN EQUATIONS*

Haoning Dang
School of Mathematics, Jilin University, Changchun 130012, China
Email: danghn9918@mails.jlu.edu.cn
Hui Peng
School of Mathematical Sciences and MOE-LSC, Shanghai Jiao Tong University, Shanghai 200240, China
Email: penghui23@sjtu.edu.cn
Qilong Zhai[1)]
School of Mathematics, Jilin University, Changchun 130012, China
Email: zhaiql@jlu.edu.cn
Ran Zhang
School of Mathematics, Jilin University, Changchun 130012, China
Email: zhangran@jlu.edu.cn

Abstract

We develop a stabilizer free weak Galerkin (SFWG) finite element method for Brinkman equations. The main idea is to use high order polynomials to compute the discrete weak gradient and then the stabilizing term is removed from the numerical formulation. The SFWG scheme is very simple and easy to implement on polygonal meshes. We prove the well-posedness of the scheme and derive optimal order error estimates in energy and L^2 norm. The error results are independent of the permeability tensor, hence the SFWG method is stable and accurate for both the Stokes and Darcy dominated problems. Finally, we present some numerical experiments to verify the efficiency and stability of the SFWG method.

Mathematics subject classification: 65N30, 65N15.
Key words: Brinkman equations, Weak Galerkin method, Stabilizer free, Discrete weak differential operators.

1. Introduction

In this paper, we consider the following Brinkman model: Seek unknown fluid velocity $\mathbf{u}$ and pressure p satisfying

$$-\mu\Delta\mathbf{u} + \mu\kappa^{-1}\mathbf{u} + \nabla p = \mathbf{f} \quad \text{in } \Omega, \tag{1.1}$$

$$\nabla\cdot\mathbf{u} = 0 \quad \text{in } \Omega, \tag{1.2}$$

$$\mathbf{u} = \mathbf{g} \quad \text{on } \partial\Omega, \tag{1.3}$$

where $\Omega \in \mathbb{R}^d$ is a polygonal ($d=2$) or polyhedral domain ($d=3$), μ is the fluid viscosity coefficient and κ denotes the permeability tensor of the porous medium, $\mathbf{f}$ represents the momentum source term, and the boundary value $\mathbf{g}$ satisfies the compatibility condition $\int_{\partial\Omega}\mathbf{g}\cdot\mathbf{n} = 0$.

* Received November 25, 2022 / Revised version received April 6, 2023 / Accepted July 26, 2023 / Published online December 11, 2023 /
1) Corresponding author

For simplicity, we consider the Brinkman equations with boundary condition $\mathbf{g} = \mathbf{0}$ and take the viscosity coefficient μ to be 1. Assume that the permeability κ is piecewise constant and there exist two constants $\lambda_1, \lambda_2 > 0$ such that

$$\lambda_1 \xi^t \xi \leq \xi^t \kappa^{-1} \xi \leq \lambda_2 \xi^t \xi, \quad \forall \xi \in \mathbb{R}^d,$$

where ξ is a column vector and ξ^t is the transpose of ξ. We consider that λ_1 is the unit size and λ_2 may be the case of large size.

The Brinkman equations (1.1)-(1.3) can be seen as a modified version of Darcy's law obtained by adding viscous forces to the Navier-Stokes equations [5]. This model has been applied in many fields, such as power engineering, petroleum industry, geology, geophysics, and so on [4, 9, 10, 20]. Mathematically speaking, the Brinkman equations have different properties due to the varying permeability tensor κ. When κ is very large, the Brinkman equations are similar to Stokes equations. Conversely, when κ is small and close to zero, the equations are similar to Darcy equations. Therefore, the numerical method designed for Brinkman equations should be efficient and stable for both the Stokes and Darcy equations. To achieve this goal, one natural attempt is to directly apply the existing stable Stokes elements (e.g. Mini-element, $P_2 - P_0$ element, nonconforming Crouzeix-Raviart element) or the stable Darcy element (e.g. Raviart-Thomas element) to the Brinkman equations. However, numerical experiments in [22] show that when applying stable Darcy element the convergence would deteriorate when κ is relatively large and vice versa. To overcome this difficulty, many recent studies have attempted to develop suitable modified elements for Brinkman equations. For instance, Burman *et al.* [6] add stabilizing terms penalizing the jumps on the normal component of the velocity field. Juntunen *et al.* [15] generalize the classical Mini-element, and obtain a stable finite element method for varying permeability. An $H(\mathrm{div})$-conforming element is applied to a geometric multi-grid method [16] based on the DG method. In recent years, some new numerical approaches have been developed for Brinkman equations, for example, virtual element methods [7], hybridizable discontinuous Galerkin method [18, 19], mixed discontinuous Galerkin method [28], weak Galerkin methods [14, 24, 36], and so on.

The weak Galerkin (WG) finite element method is first proposed by Wang and Ye [29] for the second-order elliptic equations. They introduced the weak differential operators to approximate the classical differential operators in the variational form. A unified study on WG methods with other discontinuous Galerkin methods for solving partial differential equations has been presented in [11, 12]. The discrete weak gradient is computed by the RT_k or BDM_k elements, which limits the finite element partition to triangular meshes. In order to extend the partition to polygonal meshes, a stabilizing term is added to the WG scheme in [30]. This stabilized WG finite element method has been applied to various equations, see [13, 21, 23, 25–27, 31, 32]. However, such a stabilizing term also increases the difficulty of theoretical analysis and the complexity of algorithm implementation. Therefore, efforts have been made to remove the stabilizing term from the numerical scheme. A popular and efficient strategy is to raise the degree of the polynomial that approximates the weak gradient [33]. The specific degree of polynomial depends on the number of edges of polygonal meshes. Such a stabilizer free WG method has been applied to Stokes equations [8], parabolic equations [2,37], wave equations [17], biharmonic equations [34], and so on.

The purpose of this paper is to establish a stabilizer free weak Galerkin (SFWG) method for Brinkman equations. Adopting high order piecewise polynomial space to approximate the weak gradient of velocity, we establish a simple numerical scheme on general polygonal meshes without any stabilizing term. Furthermore, we prove the well-posedness of the numerical scheme and derive the optimal order error estimates. The corresponding energy and L^2 error estimates are independent of the permeability κ, so the SFWG method is suitable for both the Stokes and Darcy dominated problems. Besides, in programming, the calculation of the stiffness matrix is simpler and more intuitive since there is no stabilizing term.

The outline of the paper is summarized as follows. In Section 2, we introduce some basic notations and the weak formulation of Brinkman model. Section 3 is devoted to constructing the SFWG scheme. Its well-posedness is proved in Section 4. In Section 5, we derive the error equations for the numerical scheme. And we obtain the error estimates in Section 6. Finally, in Section 7, we present some numerical experiments to validate the theoretical results.

2. Preliminary

Consider an open bounded domain D with Lipschitz continuous boundary in $\mathbb{R}^d$ $(d = 2,\ 3)$. For the Sobolev spaces, we use the notations commonly used [1], such as $H^k(D)(k \geq 0)$, inner product $(\cdot\,,\cdot)_{k,D}$, norm $\|\cdot\|_{k,D}$, and semi-norm $|\cdot|_{k,D}$. In addition, the inner product defined on ∂D denotes by $\langle\cdot\,,\cdot\rangle_{k,\partial D}$. When $D = \Omega$ and $k = 0$, the subscripts D and k in the norm and inner product notations are omitted. In particular, we define the function spaces as follows:

$$
\begin{aligned}
&[H_0^1(D)]^d = \left\{\mathbf{u} \in [H^1(D)]^d : \mathbf{u}|_{\partial D} = 0\right\},\\
&L_0^2(D) = \left\{p \in L^2(D), \int_D p dx = 0\right\}.
\end{aligned}
$$

The space $H(\mathrm{div}; D)$ is defined as

$$
H(\mathrm{div}; D) = \left\{\mathbf{u} \in [L^2(D)]^d : \nabla\cdot\mathbf{u} \in L^2(D)\right\},
$$

which is equipped with the norm

$$
\|\mathbf{u}\|_{H(\mathrm{div};D)} = \left(\|\mathbf{u}\|_D^2 + \|\nabla\cdot\mathbf{u}\|_D^2\right)^{\frac{1}{2}}.
$$

The weak formulation for the Brinkman equations (1.1)-(1.3) is to find the unknown functions $\mathbf{u} \in [H_0^1(\Omega)]^d$ and $p \in L_0^2(\Omega)$ satisfying

$$
(\nabla\mathbf{u}, \nabla\mathbf{v}) + (\kappa^{-1}\mathbf{u}, \mathbf{v}) - (\nabla\cdot\mathbf{v}, p) = (\mathbf{f}, \mathbf{v}), \tag{2.1}
$$

$$
(\nabla\cdot\mathbf{u}, q) = 0 \tag{2.2}
$$

for all $\mathbf{v} \in [H_0^1(\Omega)]^d$ and $q \in L_0^2(\Omega)$.

3. A Stabilizer Free WG Finite Element Scheme

In this section, we introduce discrete weak differential operators and construct a stabilizer free WG finite element scheme.

Divide the domain Ω into polygons $(d = 2)$ or polyhedrons $(d = 3)$ satisfying the shape regular assumptions in [30]. Let $\mathcal{T}_h$ be the partition above and $\mathcal{E}_h$ be the set of all edges or faces in the partition. Denote the collection of edges or faces located inside the domain Ω by the set $\mathcal{E}_h^0 = \mathcal{E}_h\backslash\partial\Omega$. For each $T \in \mathcal{T}_h, e \in \mathcal{E}_h$, denote by h_T and h_e the diameter of T and e, respectively. The size of $\mathcal{T}_h$ is $h = \max_{T\in\mathcal{T}_h} h_T$. For a given integer $k \geq 1$, denote by $\rho \in P_k(T)$ that $\rho|_T$ is polynomial with degree no more than k.

We define the discrete weak function space for the vector-valued functions as

$$V_h = \left\{ \mathbf{v} = \{\mathbf{v}_0, \mathbf{v}_b\} : \{\mathbf{v}_0, \mathbf{v}_b\}|_T \in [P_k(T)]^d \times [P_k(e)]^d, \ \forall T \in \mathcal{T}_h, e \subset \partial T \right\}.$$

Here, $\mathbf{v}_0$ can be regarded as the value of $\mathbf{v}$ inside the cell T and $\mathbf{v}_b$ can be regarded as the value of $\mathbf{v}$ on the boundary of the cell T. Just to be clear, $\mathbf{v}_b$ defined on $e \in \mathcal{E}_h$ has only a single value. We define a subspace of V_h as

$$V_h^0 = \{\mathbf{v} : \mathbf{v} \in V_h, \mathbf{v}_b = \mathbf{0} \text{ on } \partial\Omega\}.$$

For the scalar-valued functions, we define

$$W_h = \left\{ q : q \in L_0^2(\Omega), q|_T \in P_{k-1}(T) \right\}.$$

Then we recall the definitions of the discrete weak gradient operator and the discrete weak divergence operator in [8]. For a vector-valued function

$$\mathbf{v} = \{\mathbf{v}_0, \mathbf{v}_b\} \in V_h + [H^1(\Omega)]^d,$$

the discrete weak gradient $\nabla_w \mathbf{v}$ is a unique polynomial function in $[P_j(T)]^{d\times d}$ $(j > k)$ on each cell T satisfying

$$(\nabla_w \mathbf{v}, \iota)_T = -(\mathbf{v}_0, \nabla \cdot \iota)_T + \langle \mathbf{v}_b, \iota \cdot \mathbf{n} \rangle_{\partial T}, \quad \forall \iota \in [P_j(T)]^{d\times d}, \tag{3.1}$$

where $\mathbf{n}$ is the unit outward normal vector to ∂T. We remark that $j = n_e + k - 1$, n_e is the number of edges of polygon T [33]. In particular, we have $j = k + 1$, when the domain is partitioned into triangles [3].

The discrete weak divergence $\nabla_w \cdot \mathbf{v}$ is a unique polynomial function in $P_{k-1}(T)$ on each cell T satisfying

$$(\nabla_w \cdot \mathbf{v}, \rho)_T = -(\mathbf{v}_0, \nabla \rho)_T + \langle \mathbf{v}_b, q\mathbf{n} \rangle_{\partial T}, \quad \forall \rho \in P_{k-1}(T). \tag{3.2}$$

We are now in the position to construct an SFWG numerical scheme for (1.1)-(1.3). For simplicity of notations, we introduce two bilinear forms $a(\cdot\,,\cdot)$ and $b(\cdot\,,\cdot)$ as follows:

$$\begin{aligned} a(\mathbf{v}, \mathbf{w}) &= (\nabla_w \mathbf{v}, \nabla_w \mathbf{w}) + (\kappa^{-1}\mathbf{v}_0, \mathbf{w}_0), \\ b(\mathbf{v}, q) &= (\nabla_w \cdot \mathbf{v}, q). \end{aligned}$$

With these preparations, we give the SFWG numerical scheme.

Algorithm 3.1: SFWG Numerical Scheme.

Find $\mathbf{u}_h = \{\mathbf{u}_0, \mathbf{u}_b\} \in V_h^0$ and $p_h \in W_h$ such that

$$(\nabla_w \mathbf{u}_h, \nabla_w \mathbf{v}) + (\kappa^{-1}\mathbf{u}_0, \mathbf{v}_0) - (\nabla_w \cdot \mathbf{v}, p_h) = (\mathbf{f}, \mathbf{v}_0), \tag{3.3}$$

$$(\nabla_w \cdot \mathbf{u}_h, q) = 0 \tag{3.4}$$

for all $\mathbf{v} = \{\mathbf{v}_0, \mathbf{v}_b\} \in V_h^0$ and $q \in W_h$.

4. Stability and Solvability

In order to discuss the well-posedness of SFWG scheme, we first define a tri-bar norm. For any $\mathbf{v} = \{\mathbf{v}_0, \mathbf{v}_b\} \in V_h + [H^1(\Omega)]^d$,

$$|\!|\!|\mathbf{v}|\!|\!|^2 = a(\mathbf{v}, \mathbf{v}) = \|\nabla_w \mathbf{v}\|^2 + \left\|\kappa^{-\frac{1}{2}} \mathbf{v}_0\right\|^2. \tag{4.1}$$

We also need another discrete H^1 norm $\|\cdot\|_{1,h}$ in V_h^0 given by [24]

$$\|\mathbf{v}\|_{1,h}^2 = \|\nabla_w \mathbf{v}\|^2 + \sum_{T\in\mathcal{T}_h} h_T^{-1} \|\mathbf{v}_0 - \mathbf{v}_b\|_{\partial T}^2. \tag{4.2}$$

For any $q \in W_h$, we use the following norm $|\!|\!|\cdot|\!|\!|_1$ in the rest of this paper:

$$|\!|\!|q|\!|\!|_1^2 = \sum_{T\in\mathcal{T}_h} \left\|\kappa^{\frac{1}{2}} \nabla q\right\|_T^2 + h^{-1} \sum_{e\in\mathcal{E}_h^0} \|\lceil q \rceil\|_e^2, \tag{4.3}$$

where $\lceil q \rceil$ is defined as follows: If $e \subset \mathcal{E}_h^0$ is shared by T_1 and T_2, and $\mathbf{n}_1$ and $\mathbf{n}_2$ are the unit outward normal vectors of T_1 and T_2 to e, then denote by $\lceil q \rceil = q|_{T_1}\mathbf{n}_1 + q|_{T_2}\mathbf{n}_2$.

Lemma 4.1 ([8, Lemma 4.1]). *For any $\mathbf{v} = \{\mathbf{v}_0, \mathbf{v}_b\} \in V_h$ and $T \in \mathcal{T}_h$, it holds*

$$h_T^{-1} \|\mathbf{v}_0 - \mathbf{v}_b\|_{\partial T}^2 \le C \|\nabla_w \mathbf{v}\|_T^2, \tag{4.4}$$

where C is a positive constant.

According to (4.2) and Lemma 4.1, over all cell T, then it is straightforward to show that

$$\|\mathbf{v}\|_{1,h}^2 \le C \|\nabla_w \mathbf{v}\|^2 \le C |\!|\!|\mathbf{v}|\!|\!|^2. \tag{4.5}$$

Lemma 4.2. *$|\!|\!|\cdot|\!|\!|$ defined in (4.1) provides a norm in V_h.*

Proof. It is obvious that $|\!|\!|\cdot|\!|\!|$ defines a semi-norm in V_h. Then, assume $|\!|\!|\mathbf{v}|\!|\!| = 0$ for a $\mathbf{v} \in V_h$, we have

$$\|\nabla_w \mathbf{v}\|^2 + \left\|\kappa^{-\frac{1}{2}} \mathbf{v}_0\right\|^2 = 0,$$

which implies $\nabla_w \mathbf{v} = \mathbf{0}$ and $\mathbf{v}_0 = \mathbf{0}$ on each cell. According to (4.4), we obtain $\mathbf{v}_0 = \mathbf{v}_b = \mathbf{0}$, which completes the proof. ☐

From the definition of the norm $|\!|\!|\cdot|\!|\!|$ and the Cauchy-Schwarz inequality, the following lemma holds true.

Lemma 4.3. *For any $\mathbf{v}, \mathbf{w} \in V_h$, we have*

$$|a(\mathbf{v}, \mathbf{w})| \le |\!|\!|\mathbf{v}|\!|\!| \, |\!|\!|\mathbf{w}|\!|\!|.$$

Lemma 4.4. *For any nonzero $q \in W_h$, let $F(q) = \{-\kappa \nabla q, h^{-1} \lceil q \rceil \mathbf{n}_e\}$ be the artificial flux of q (see [24]), we have*

$$\frac{b\big(F(q), q\big)}{|\!|\!|q|\!|\!|_1} = |\!|\!|q|\!|\!|_1. \tag{4.6}$$

Furthermore, there exists a positive constant C such that

$$\|F(q)\|_{1,h} \le C h^{-1} |\!|\!|q|\!|\!|_1. \tag{4.7}$$

Proof. (4.6) can be verified directly by the definition of $|\!|\!| \cdot |\!|\!|_1$. We only need to prove the estimate (4.7). From the proof [24, Lemma 3.2], we have

$$\|\nabla_w F(q)\|^2 \le Ch^{-2} |\!|\!| q |\!|\!|_1^2.$$

Taking $\mathbf{v} = F(q)$ in (4.5), we obtain

$$\|F(q)\|_{1,h}^2 \le C\|\nabla_w F(q)\|^2.$$

Combining the estimates above, we complete the proof of (4.7). □

Lemma 4.4 yields the following inf-sup condition:

$$\sup_{\mathbf{v}\in V_h} \frac{b(\mathbf{v}, q)}{\|\mathbf{v}\|_{1,h}} \ge Ch |\!|\!| q |\!|\!|_1, \quad \forall\, q \in W_h. \tag{4.8}$$

Lemma 4.5. *The stabilizer free weak Galerkin finite element scheme* (3.3)-(3.4) *has a unique solution.*

Proof. Consider the corresponding homogeneous equation $\mathbf{f} = \mathbf{0}$, let $\mathbf{v} = \mathbf{u}_h$ in (3.3) and $q = p_h$ in (3.4). Subtracting these two equations, we have

$$|\!|\!| \mathbf{u}_h |\!|\!|^2 = a(\mathbf{u}_h, \mathbf{u}_h) = 0,$$

which implies $\mathbf{u}_h = \mathbf{0}$.

Taking $\mathbf{v} = F(p_h)$, where $F(\cdot)$ is defined in Lemma 4.4. It follows from $\mathbf{u}_h = \mathbf{0}$ and $\mathbf{f} = \mathbf{0}$ that

$$0 = b\big(F(p_h), p_h\big) = |\!|\!| p_h |\!|\!|_1^2. \tag{4.9}$$

Thus, $p_h = 0$ and we obtain the solvability of SFWG scheme. □

5. Error Equations

In this section, we derive the equations of the error between the numerical solution and the exact solution. For each $T \in \mathcal{T}_h$, let $Q_h, \mathbf{Q}_h$ and $\mathbb{Q}_h$ be the L^2 projection operators onto $[P_k(T)]^d, [P_j(T)]^{d\times d}$ and $P_{k-1}(T)$ defined in [8]. First, we recall the commutative properties of the projection operators.

Lemma 5.1 ([8]). *For the projection operators $Q_h, \mathbf{Q}_h$ and $\mathbb{Q}_h$, the following properties hold true:*

$$\begin{aligned} &\nabla_w \cdot (Q_h \mathbf{v}) = \mathbb{Q}_h(\nabla \cdot \mathbf{v}), && \forall\, \mathbf{v} \in H(\mathrm{div}; \Omega), \\ &\nabla_w \mathbf{v} = \mathbf{Q}_h(\nabla \mathbf{v}), && \forall\, \mathbf{v} \in [H^1(\Omega)]^d. \end{aligned}$$

Let $\mathbf{u}$ and p be the exact solution of Brinkman equations (1.1)-(1.3), $\mathbf{u}_h = \{\mathbf{u}_0, \mathbf{u}_b\}$ and p_h be the numerical solution of SFWG algorithm (3.3)-(3.4). Define

$$\mathbf{e}_h = \{\mathbf{e}_0, \mathbf{e}_b\} = \{Q_0\mathbf{u} - \mathbf{u}_0, Q_b\mathbf{u} - \mathbf{u}_b\} = Q_h\mathbf{u} - \mathbf{u}_h, \quad \varepsilon_h = \mathbb{Q}_h p - p_h$$

be the error functions, we shall derive the error equations for $\mathbf{e}_h$ and ε_h.

Lemma 5.2. *For any $\mathbf{v}=\{\mathbf{v}_0,\mathbf{v}_b\}\in V_h^0$ and $q\in W_h$, the following equations hold true:*

$$a(\mathbf{e}_h,\mathbf{v})-b(\mathbf{v},\varepsilon_h)=l_1(\mathbf{u},\mathbf{v})-l_2(p,\mathbf{v})-l_3(\mathbf{u},\mathbf{v}), \tag{5.1}$$
$$b(\mathbf{e}_h,q)=0, \tag{5.2}$$

where

$$\begin{aligned}
l_1(\mathbf{u},\mathbf{v}) &= \sum_{T\in\mathcal{T}_h}\langle(\nabla\mathbf{u}-\mathbf{Q}_h\nabla\mathbf{u})\cdot\mathbf{n},\mathbf{v}_0-\mathbf{v}_b\rangle_{\partial T},\\
l_2(p,\mathbf{v}) &= \sum_{T\in\mathcal{T}_h}\langle(p-\mathbb{Q}_hp)\mathbf{n},\mathbf{v}_0-\mathbf{v}_b\rangle_{\partial T},\\
l_3(\mathbf{u},\mathbf{v}) &= \sum_{T\in\mathcal{T}_h}\big(\nabla_w(\mathbf{u}-Q_h\mathbf{u}),\nabla_w\mathbf{v}_h\big)_T.
\end{aligned}$$

Proof. Testing (1.1) by $\mathbf{v}_0$ gives

$$-(\Delta\mathbf{u},\mathbf{v}_0)+\big(\kappa^{-1}\mathbf{u},\mathbf{v}_0\big)+(\nabla p,\mathbf{v}_0)=(\mathbf{f},\mathbf{v}_0).$$

By the definitions of projection operators Q_h and $\mathbf{Q}_h$, the definitions of the weak differential operators ∇_w and $\nabla_w\cdot$, and Lemma 5.1, we get

$$\begin{aligned}
-(\Delta\mathbf{u},\mathbf{v}_0) &= \sum_{T\in\mathcal{T}_h}\big((\nabla\mathbf{u},\nabla\mathbf{v}_0)_T-\langle\nabla\mathbf{u}\cdot\mathbf{n},\mathbf{v}_0\rangle_{\partial T}\big)\\
&= \sum_{T\in\mathcal{T}_h}\big((\mathbf{Q}_h\nabla\mathbf{u},\nabla\mathbf{v}_0)_T-\langle\nabla\mathbf{u}\cdot\mathbf{n},\mathbf{v}_0\rangle_{\partial T}\big)\\
&= \sum_{T\in\mathcal{T}_h}\big(-\big(\mathbf{v}_0,\nabla\cdot(\mathbf{Q}_h\nabla\mathbf{u})\big)_T+\langle\mathbf{v}_0,(\mathbf{Q}_h\nabla\mathbf{u}-\nabla\mathbf{u})\cdot\mathbf{n}\rangle_{\partial T}\big)\\
&= \sum_{T\in\mathcal{T}_h}\big((\nabla_w\mathbf{v}_h,\mathbf{Q}_h\nabla\mathbf{u})_T+\langle\mathbf{v}_0-\mathbf{v}_b,(\mathbf{Q}_h\nabla\mathbf{u}-\nabla\mathbf{u})\cdot\mathbf{n}\rangle_{\partial T}\big)\\
&= \sum_{T\in\mathcal{T}_h}\big((\nabla_w\mathbf{v}_h,\nabla_w\mathbf{u})_T+\langle\mathbf{v}_0-\mathbf{v}_b,(\mathbf{Q}_h\nabla\mathbf{u}-\nabla\mathbf{u})\cdot\mathbf{n}\rangle_{\partial T}\big).
\end{aligned}$$

From the definition of $l_1(\cdot,\cdot)$ and $l_3(\cdot,\cdot)$, it follows that

$$-(\Delta\mathbf{u},\mathbf{v}_0)=\sum_{T\in\mathcal{T}_h}\big(\nabla_w\mathbf{v}_h,\nabla_w(Q_h\mathbf{u})\big)_T-l_1(\mathbf{u},\mathbf{v})+l_3(\mathbf{u},\mathbf{v}). \tag{5.3}$$

Similarly, we have

$$\begin{aligned}
(\nabla p,\mathbf{v}_0) &= -\sum_{T\in\mathcal{T}_h}(\mathbb{Q}_hp,\nabla_w\cdot\mathbf{v}_h)_T+l_2(p,\mathbf{v}),\\
\big(\kappa^{-1}\mathbf{u},\mathbf{v}_0\big) &= \big(\mathbf{u},\kappa^{-1}\mathbf{v}_0\big)=\big(Q_0\mathbf{u},\kappa^{-1}\mathbf{v}_0\big)=\big(\kappa^{-1}Q_0\mathbf{u},\mathbf{v}_0\big).
\end{aligned}$$

Using the definition of $a(\cdot,\cdot)$ and $b(\cdot,\cdot)$ and the above equations, we obtain

$$a(Q_h\mathbf{u},\mathbf{v})-b(\mathbf{v},\mathbb{Q}_hp)-l_1(\mathbf{u},\mathbf{v})+l_2(p,\mathbf{v})+l_3(\mathbf{u},\mathbf{v})=(\mathbf{f},\mathbf{v}_0). \tag{5.4}$$

Since the numerical solution $(\mathbf{u}_h;p_h)\in V_h^0\times W_h$ satisfies (3.3), subtracting it from (5.4), we arrive at

$$a(\mathbf{e}_h,\mathbf{v})-b(\mathbf{v},\varepsilon_h)-l_1(\mathbf{u},\mathbf{v})+l_2(p,\mathbf{v})+l_3(\mathbf{u},\mathbf{v})=0,$$

which completes the proof of (5.1).

Similarly, testing (1.2) by $q \in W_h$ yields

$$0 = (\nabla \cdot \mathbf{u}, q) = \big(\mathbb{Q}_h(\nabla \cdot \mathbf{u}), q\big) = \big(\nabla_w \cdot (Q_h\mathbf{u}), q\big) = b(Q_h\mathbf{u}, q). \tag{5.5}$$

Combining with (3.4), we obtain (5.2) and complete the proof of this lemma. □

6. Error Estimates

The goal of this section is to present the error results of the numerical scheme (3.3)-(3.4). Firstly, we discuss the error estimate in the energy norm.

Theorem 6.1. *Let $(\mathbf{u}; p) \in [H_0^1(\Omega) \cap H^{k+1}(\Omega)]^d \times (L_0^2(\Omega) \cap H^k(\Omega))$ be the exact solution of Brinkman equations (1.1)-(1.3) and $(\mathbf{u}_h; p_h) \in V_h^0 \times W_h$ be the solution of (3.3)-(3.4). Then, there exists a constant C such that*

$$|||\mathbf{e}_h||| + h|||\varepsilon_h|||_1 \le Ch^k(\|\mathbf{u}\|_{k+1} + \|p\|_k). \tag{6.1}$$

Proof. Letting $\mathbf{v} = \mathbf{e}_h$ in (5.1) and $q = \varepsilon_h$ in (5.2), then adding the two equations, we have

$$|||\mathbf{e}_h|||^2 = l_1(\mathbf{u}, \mathbf{e}_h) - l_2(p, \mathbf{e}_h) - l_3(\mathbf{u}, \mathbf{e}_h).$$

From the estimates (A.6)-(A.8), we obtain

$$|||\mathbf{e}_h|||^2 \le Ch^k(\|\mathbf{u}\|_{k+1} + \|p\|_k)|||\mathbf{e}_h|||.$$

The derivation of the pressure estimate is similar to that in [24], which is

$$h|||\varepsilon_h|||_1 \le Ch^k(\|\mathbf{u}\|_{k+1} + \|p\|_k),$$

which gives estimate of $|||\varepsilon_h|||_1$. The proof is complete. □

In order to derive L^2 error estimate for the velocity, we consider the following dual problem: Find $(\boldsymbol{\phi}; \eta) \in [H^2(\Omega)]^d \times H^1(\Omega)$ satisfying

$$-\Delta\boldsymbol{\phi} + \kappa^{-1}\boldsymbol{\phi} + \nabla\eta = \mathbf{e}_0 \quad \text{in } \Omega, \tag{6.2}$$

$$\nabla \cdot \boldsymbol{\phi} = 0 \quad \text{in } \Omega, \tag{6.3}$$

$$\boldsymbol{\phi} = \mathbf{0} \quad \text{on } \partial\Omega. \tag{6.4}$$

Assume that the following regularity condition holds:

$$\|\boldsymbol{\phi}\|_2 + \|\eta\|_1 \le C\|\mathbf{e}_0\|. \tag{6.5}$$

Theorem 6.2. *Let $(\mathbf{u}; p) \in [H_0^1(\Omega) \cap H^{k+1}(\Omega)]^d \times (L_0^2(\Omega) \cap H^k(\Omega))$ be the exact solution of Brinkman equations (1.1)-(1.3) and $(\mathbf{u}_h; p_h) \in V_h^0 \times W_h$ be the solution of (3.3)-(3.4). Then, there exists a constant C such that*

$$\|\mathbf{e}_0\| \le Ch^{k+1}(\|\mathbf{u}\|_{k+1} + \|p\|_k). \tag{6.6}$$

Proof. Testing (6.2) by $\mathbf{e}_0$, we get

$$\|\mathbf{e}_0\|^2 = (\mathbf{e}_0, \mathbf{e}_0) = -(\Delta\boldsymbol{\phi}, \mathbf{e}_0) + (\kappa^{-1}\boldsymbol{\phi}, \mathbf{e}_0) + (\nabla\eta, \mathbf{e}_0). \tag{6.7}$$

According to the proof of Lemma 5.2, it is easy to derive that

$$
\begin{aligned}
-(\Delta\boldsymbol{\phi}, \mathbf{e}_0) &= \sum_{T\in\mathcal{T}_h} \big(\nabla_w \mathbf{e}_h, \nabla_w(Q_h\boldsymbol{\phi})\big)_T - l_1(\boldsymbol{\phi}, \mathbf{e}_h) + l_3(\boldsymbol{\phi}, \mathbf{e}_h),\\
(\nabla\eta, \mathbf{e}_0) &= -\sum_{T\in\mathcal{T}_h} (\mathbb{Q}_h\eta, \nabla_w\cdot\mathbf{e}_h)_T + l_2(\eta, \mathbf{e}_h).
\end{aligned}
$$

It follows from the Eqs. (5.2) and (6.3) that

$$
b(\mathbf{e}_h, \mathbb{Q}_h\eta) = 0, \quad b(Q_h\boldsymbol{\phi}, \varepsilon_h) = 0.
$$

Substituting these two equations into (6.7), we arrive at

$$
\begin{aligned}
\|\mathbf{e}_0\|^2 &= a(Q_h\boldsymbol{\phi}, \mathbf{e}_h) - b(\mathbf{e}_h, \mathbb{Q}_h\eta) - l_1(\boldsymbol{\phi}, \mathbf{e}_h) + l_2(\eta, \mathbf{e}_h) + l_3(\boldsymbol{\phi}, \mathbf{e}_h)\\
&= a(Q_h\boldsymbol{\phi}, \mathbf{e}_h) - b(Q_h\boldsymbol{\phi}, \varepsilon_h) - l_1(\boldsymbol{\phi}, \mathbf{e}_h) + l_2(\eta, \mathbf{e}_h) + l_3(\boldsymbol{\phi}, \mathbf{e}_h).
\end{aligned}
$$

Taking $\mathbf{v} = Q_h\boldsymbol{\phi}$ in Lemma 5.2 yields

$$
\|\mathbf{e}_0\|^2 = l_1(\mathbf{u}, Q_h\boldsymbol{\phi}) - l_2(p, Q_h\boldsymbol{\phi}) - l_3(\mathbf{u}, Q_h\boldsymbol{\phi}) - \big(l_1(\boldsymbol{\phi}, \mathbf{e}_h) - l_2(\eta, \mathbf{e}_h) - l_3(\boldsymbol{\phi}, \mathbf{e}_h)\big).
$$

Next, we estimate the terms on the right-hand side of the above equation one by one. It follows from Lemma A.3 that

$$
|l_1(\boldsymbol{\phi}, \mathbf{e}_h) - l_2(\eta, \mathbf{e}_h) - l_3(\boldsymbol{\phi}, \mathbf{e}_h)| \le Ch(\|\boldsymbol{\phi}\|_2 + \|\eta\|_1)|\!|\!|\mathbf{e}_h|\!|\!|.
$$

For $l_1(\mathbf{u}, Q_h\boldsymbol{\phi})$, using the definition of Q_b, the trace inequality (A.4) and the projection inequalities (A.1)-(A.2) gives

$$
\begin{aligned}
|l_1(\mathbf{u}, Q_h\boldsymbol{\phi})| &= \left| \sum_{T\in\mathcal{T}_h} \langle (\nabla\mathbf{u} - \mathbf{Q}_h\nabla\mathbf{u})\cdot\mathbf{n}, Q_0\boldsymbol{\phi} - Q_b\boldsymbol{\phi}\rangle_{\partial T} \right|\\
&\le C\left(\sum_{T\in\mathcal{T}_h} h_T\|\nabla\mathbf{u} - \mathbf{Q}_h\nabla\mathbf{u}\|_{\partial T}^2\right)^{\frac{1}{2}} \left(\sum_{T\in\mathcal{T}_h} h_T^{-1}\|Q_0\boldsymbol{\phi} - Q_b\boldsymbol{\phi}\|_{\partial T}^2\right)^{\frac{1}{2}}\\
&\le C\left(\sum_{T\in\mathcal{T}_h} h_T\|\nabla\mathbf{u} - \mathbf{Q}_h\nabla\mathbf{u}\|_{\partial T}^2\right)^{\frac{1}{2}} \left(\sum_{T\in\mathcal{T}_h} h_T^{-1}\|Q_0\boldsymbol{\phi} - \boldsymbol{\phi}\|_{\partial T}^2\right)^{\frac{1}{2}}\\
&\le Ch^{k+1}\|\mathbf{u}\|_{k+1}\|\boldsymbol{\phi}\|_2.
\end{aligned}
$$

Similarly, we have

$$
\begin{aligned}
|l_2(p, Q_h\boldsymbol{\phi})| &= \left| \sum_{T\in\mathcal{T}_h} \langle (p - \mathbb{Q}_h p)\mathbf{n}, Q_0\boldsymbol{\phi} - Q_b\boldsymbol{\phi}\rangle_{\partial T} \right|\\
&\le Ch^{k+1}\|p\|_k\|\boldsymbol{\phi}\|_2.
\end{aligned}
$$

Finally, we estimate $l_3(\mathbf{u}, Q_h\boldsymbol{\phi})$. Besides the projection operators defined in the previous section, we need another L^2 projection operator. Denote by $\hat{\mathbf{Q}}_h$ the projection operator from $[L^2(T)]^{d\times d}$ onto $[P_1(T)]^{d\times d}$. For any $q \in P_1(T)$, we have

$$
\big(\hat{\mathbf{Q}}_h\nabla\boldsymbol{\phi}, q\big)_T = (\nabla\boldsymbol{\phi}, q)_T = -(\boldsymbol{\phi}, \nabla\cdot q)_T + \langle\boldsymbol{\phi}, q\mathbf{n}\rangle_{\partial T} = (\nabla_w\boldsymbol{\phi}, q)_T = \big(\hat{\mathbf{Q}}_h\nabla_w\boldsymbol{\phi}, q\big)_T,
$$

which implies $\hat{\mathbf{Q}}_h\nabla\boldsymbol{\phi} = \hat{\mathbf{Q}}_h\nabla_w\boldsymbol{\phi}$ on each cell T. Then, according to the definition of ∇_w and the fact that $k \geq 1$, we have

$$\begin{aligned}
&\big(\nabla_w(\mathbf{u}-Q_h\mathbf{u}), \hat{\mathbf{Q}}_h\nabla\boldsymbol{\phi}\big)_T\\
=&\big(\nabla_w(\mathbf{u}-Q_h\mathbf{u}), \hat{\mathbf{Q}}_h\nabla_w\boldsymbol{\phi}\big)_T\\
=&-\big(\mathbf{u}-Q_0\mathbf{u}, \nabla\cdot(\hat{\mathbf{Q}}_h\nabla_w\boldsymbol{\phi})\big)_T\\
&+\big\langle \mathbf{u}-Q_b\mathbf{u}, \big(\hat{\mathbf{Q}}_h\nabla_w\boldsymbol{\phi}\big)\cdot\mathbf{n}\big\rangle_{\partial T} = 0.
\end{aligned} \tag{6.8}$$

Then, using the definition of ∇_w, Eq. (6.8), the projection inequality (A.2) and the estimate (A.5), we arrive at

$$\begin{aligned}
&\sum_{T\in\mathcal{T}_h}\big(\nabla_w\boldsymbol{\phi}, \nabla_w(\mathbf{u}-Q_h\mathbf{u})\big)_T\\
=&\sum_{T\in\mathcal{T}_h}\big(\nabla\boldsymbol{\phi}, \nabla_w(\mathbf{u}-Q_h\mathbf{u})\big)_T\\
=&\sum_{T\in\mathcal{T}_h}\big(\nabla\boldsymbol{\phi}-\hat{\mathbf{Q}}_h\nabla\boldsymbol{\phi}, \nabla_w(\mathbf{u}-Q_h\mathbf{u})\big)_T\\
\leq&\left(\sum_{T\in\mathcal{T}_h}\|\nabla\boldsymbol{\phi}-\hat{\mathbf{Q}}_h\nabla\boldsymbol{\phi}\|_T^2\right)^{\frac{1}{2}}\left(\sum_{T\in\mathcal{T}_h}\|\nabla_w(\mathbf{u}-Q_h\mathbf{u})\|_T^2\right)^{\frac{1}{2}}\\
\leq& Ch^{k+1}\|\mathbf{u}\|_{k+1}\|\boldsymbol{\phi}\|_2.
\end{aligned}$$

Thus, for $l_3(\mathbf{u}, Q_h\boldsymbol{\phi})$, we get

$$\begin{aligned}
|l_3(\mathbf{u}, Q_h\boldsymbol{\phi})| &= \left|\sum_{T\in\mathcal{T}_h}\big(\nabla_w Q_h\boldsymbol{\phi}, \nabla_w(\mathbf{u}-Q_h\mathbf{u})\big)_T\right|\\
&\leq\left|\sum_{T\in\mathcal{T}_h}\big(\nabla_w(Q_h\boldsymbol{\phi}-\boldsymbol{\phi}), \nabla_w(\mathbf{u}-Q_h\mathbf{u})\big)_T\right|+\left|\sum_{T\in\mathcal{T}_h}\big(\nabla_w\boldsymbol{\phi}, \nabla_w(\mathbf{u}-Q_h\mathbf{u})\big)_T\right|\\
&\leq Ch^{k+1}\|\mathbf{u}\|_{k+1}\|\boldsymbol{\phi}\|_2.
\end{aligned}$$

Combining (6.5) and (6.1), we obtain

$$\begin{aligned}
\|\mathbf{e}_0\|^2 &\leq Ch^{k+1}(\|\mathbf{u}\|_{k+1}+\|p\|_k)\|\boldsymbol{\phi}\|_2 + Ch(\|\boldsymbol{\phi}\|_2+\|\eta\|_1)|\!|\!|\mathbf{e}_h|\!|\!|\\
&\leq Ch^{k+1}(\|\mathbf{u}\|_{k+1}+\|p\|_k)\|\mathbf{e}_0\| + Ch\|\mathbf{e}_0\||\!|\!|\mathbf{e}_h|\!|\!|\\
&\leq Ch^{k+1}(\|\mathbf{u}\|_{k+1}+\|p\|_k)\|\mathbf{e}_0\|,
\end{aligned}$$

which completes the proof of the theorem. □

7. Numerical Experiments

In this section, we present several numerical examples to verify the stability and order of convergence established in Section 6.

Example 7.1. Let $\Omega = (0,1)\times(0,1)$, the exact solution is given as follows:

$$\mathbf{u} = \begin{pmatrix} \sin(2\pi x)\cos(2\pi y)\\ -\cos(2\pi x)\sin(2\pi y)\end{pmatrix}, \quad p = x^2y^2 - \frac{1}{9}.$$

Consider the following permeability:

$$\kappa^{-1} = a\big(\sin(2\pi x) + 1.1\big),$$

where a is a given positive constant. According to the above parameters, the momentum source term $\mathbf{f}$ and the boundary value $\mathbf{g}$ can be calculated.

When $k = 1$, we use uniform triangular partition as shown in Fig. 7.1(a). Tables 7.1-7.4 show the errors and orders of convergence as $\mu = 1,\ 0.01$ and $a = 1,\ 10^4$. When $k = 2,\ 3$, we use uniform rectangular partition and polygonal partition as shown in Figs. 7.1(b) and 7.1(c). Tables 7.5-7.8 show the errors and orders of convergence as $\mu = 1$ and $a = 10^4$, we observe that the numerical experiment results are consistent with the theoretical analysis, and the optimal convergence orders are achieved. At the same time, the accuracy and stability of the numerical scheme are verified when the permeability κ is highly varying.

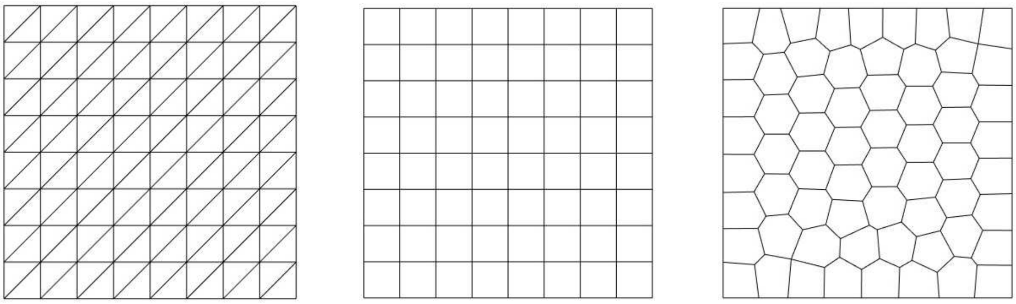

(a) Triangle partition (b) Rectangle partition (c) Arbitrary polygonal partition

Fig. 7.1. Three kinds of partitions as $h = 1/8$.

Table 7.1: Errors and orders of convergence on triangular partition as $k = 1, j = 2, \mu = 1, a = 1$.

h	$\|\!\|\!\|\mathbf{e}_h\|\!\|\!\|$	Order	$\|\mathbf{e}_h\|$	Order	$\|\varepsilon_h\|$	Order
1/4	2.1115e+00		1.0192e-01		9.9680e-01	
1/8	1.0768e-01	0.9715	3.5806e-02	1.5108	6.0078e-01	0.7305
1/16	5.3371e-01	1.0126	9.9527e-03	1.8454	3.2312e-01	0.8948
1/32	2.6577e-01	1.0059	2.5628e-03	1.9574	1.6520e-01	0.9679
1/64	1.3273e-01	1.0017	6.4563e-04	1.9889	8.3097e-02	0.9913
1/128	6.6342e-02	1.0005	1.6172e-04	1.9972	4.1613e-02	0.9978

Table 7.2: Errors and orders of convergence on triangular partition as $k = 1, j = 2, \mu = 0.01, a = 1$.

h	$\|\!\|\!\|\mathbf{e}_h\|\!\|\!\|$	Order	$\|\mathbf{e}_h\|$	Order	$\|\varepsilon_h\|$	Order
1/4	4.3216e-01		2.5544e-01		2.6404e-02	
1/8	2.3379e-01	0.8864	7.8264e-02	1.7066	1.1273e-02	1.2279
1/16	1.2018e-01	0.9599	2.1059e-02	1.8939	4.5551e-03	1.3073
1/32	6.0684e-02	0.9859	5.3940e-03	1.9650	1.9287e-03	1.2399
1/64	3.0442e-02	0.9953	1.3588e-03	1.9890	8.8154e-04	1.1297
1/128	1.5237e-02	0.9985	3.4048e-04	1.9967	4.2468e-04	1.0535

Table 7.3: Errors and orders of convergence on triangular partition as $k = 1, j = 2, \mu = 1, a = 10^4$.

h	$\|\|\|\mathbf{e}_h\|\|\|$	Order	$\|\|\mathbf{e}_h\|\|$	Order	$\|\|\varepsilon_h\|\|$	Order
1/4	2.7937e+00		3.0915e-02		8.0996e-01	
1/8	9.7644e-01	1.5165	3.9298e-03	2.9758	7.4012e-01	0.1301
1/16	5.0617e-01	0.9479	1.1969e-03	1.7152	4.4246e-01	0.7422
1/32	2.6126e-01	0.9541	3.7644e-04	1.6687	2.1493e-01	1.0417
1/64	1.3211e-01	0.9837	1.0288e-04	1.8714	9.5725e-02	1.1669
1/128	6.6263e-02	0.9954	2.6397e-05	1.9625	4.3719e-02	1.1306

Table 7.4: Errors and orders of convergence on triangular partition as $k = 1, j = 2, \mu = 0.01, a = 10^4$.

h	$\|\|\|\mathbf{e}_h\|\|\|$	Order	$\|\|\mathbf{e}_h\|\|$	Order	$\|\|\varepsilon_h\|\|$	Order
1/4	3.0356e-01		3.8087e-02		1.3871e-01	
1/8	1.4235e-01	1.0925	1.8206e-02	1.0649	1.1788e-01	0.2347
1/16	9.2281e-02	0.6254	9.7999e-03	0.8936	7.4873e-02	0.6548
1/32	5.4850e-02	0.7506	3.7480e-03	1.3867	3.3981e-02	1.1397
1/64	2.9532e-02	0.8932	1.1167e-03	1.7468	1.1297e-02	1.5888
1/128	1.5115e-02	0.9663	2.9507e-04	1.9201	3.1290e-03	1.8522

Table 7.5: Errors and orders of convergence on rectangular partition as $k = 2, j = 5, \mu = 1, a = 10^4$.

h	$\|\|\|\mathbf{e}_h\|\|\|$	Order	$\|\|\mathbf{e}_h\|\|$	Order	$\|\|\varepsilon_h\|\|$	Order
1/4	1.5090e+00		1.4271e-02		1.9516e+00	
1/8	3.9217e-01	1.9440	1.4107e-03	3.3386	2.1634e-01	3.1733
1/16	1.0623e-01	1.8843	1.8286e-04	2.9476	1.7497e-02	3.6282
1/32	2.7212e-02	1.9649	2.3592e-05	2.9544	1.5721e-03	3.4763
1/64	6.8568e-03	1.9886	2.9630e-06	2.9931	1.6816e-04	3.2248

Table 7.6: Errors and orders of convergence on rectangular partition as $k = 3, j = 6, \mu = 1, a = 10^4$.

h	$\|\|\|\mathbf{e}_h\|\|\|$	Order	$\|\|\mathbf{e}_h\|\|$	Order	$\|\|\varepsilon_h\|\|$	Order
1/4	3.3980e-01		2.7885e-03		2.2952e-01	
1/8	4.7427e-02	2.8409	2.0378e-04	3.7744	1.6021e-02	3.8405
1/16	6.5959e-03	2.8461	1.4658e-05	3.7972	1.0867e-03	3.8820
1/32	8.5343e-04	2.9502	9.6074e-07	3.9314	9.4871e-05	3.5178
1/64	1.0779e-04	2.9850	6.0620e-08	3.9863	8.3708e-06	3.5025

Table 7.7: Errors and orders of convergence on polygonal partition as $k = 2, j = 8, \mu = 1, a = 10^4$.

h	$\|\|\|\mathbf{e}_h\|\|\|$	Order	$\|\|\mathbf{e}_h\|\|$	Order	$\|\|\varepsilon_h\|\|$	Order
1/4	2.2202e+00		1.3247e-02		2.8494e+00	
1/8	5.7055e-01	1.9603	2.2613e-03	2.5504	2.9365e-01	3.2785
1/16	1.4833e-01	1.9436	3.7659e-04	2.5861	3.6338e-02	3.0145
1/32	3.7047e-02	2.0013	5.0255e-05	2.9056	5.2889e-03	2.7804
1/64	9.3813e-03	1.9815	6.3611e-06	2.9819	1.0955e-03	2.2714

Table 7.8: Errors and orders of convergence on polygonal partition as $k=3, j=9, \mu=1, a=10^4$.

h	$\|\!\|\!\|\mathbf{e}_h\|\!\|\!\|$	Order	$\|\mathbf{e}_h\|$	Order	$\|\varepsilon_h\|$	Order
1/4	4.7325e-01		2.8616e-03		2.9737e-01	
1/8	6.4970e-02	2.8647	2.1876e-04	3.7094	2.3136e-02	3.6840
1/16	7.8459e-03	3.0498	1.7711e-05	3.6266	2.2148e-03	3.3849
1/32	9.6560e-04	3.0224	1.2902e-06	3.7789	2.3085e-04	3.2622
1/64	1.1974e-04	3.0116	9.1288e-08	3.8211	2.4857e-05	3.2152

For all the above cases, we take $j=k+1$ for triangular partition and $j=n+k-1$ for other partitions which are consistent with the theoretical analysis. However, through a large number of numerical experiments, we find that in some cases, j usually does not need to reach the above value to reach the theoretical optimal convergence order. For triangular partition, $j=k+1$ is the optimal choice. For rectangular partition, $j=k+2$ is the minimum value that j can take when the optimal order convergence is achieved.

Example 7.2. We use the following data settings in Examples 7.2-7.4:

$$\Omega=(0,1)\times(0,1), \quad \mu=0.01, \quad \mathbf{f}=\begin{pmatrix}0\\0\end{pmatrix}, \quad \mathbf{g}=\begin{pmatrix}1\\0\end{pmatrix}. \tag{7.1}$$

Also, taking $k=1$ and 128×128 rectangular partition to solve the following examples.

In this example, the permeability coefficient κ is selected as the piecewise constant function with highly varying. The profile of the permeability inverse is shown in Fig. 7.2(a).

The profiles of the two components of the velocity and the pressure are plotted in Figs. 7.3(a)-7.3(c).

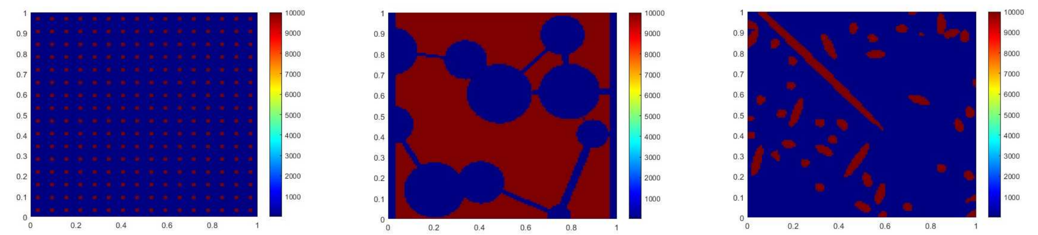

(a) Profile of κ^{-1} in Example 7.2 (b) Profile of κ^{-1} in Example 7.3 (c) Profile of κ^{-1} in Example 7.4

Fig. 7.2. Different kinds of profile of κ^{-1}.

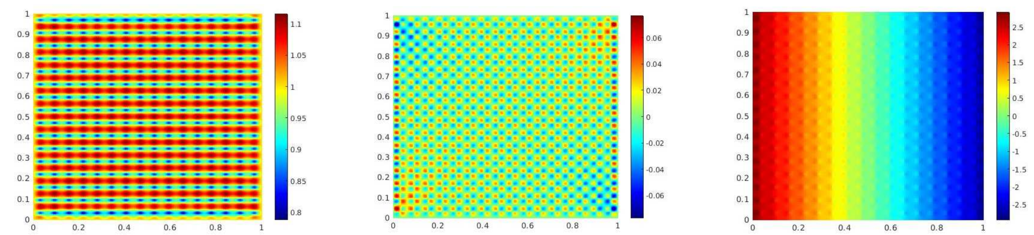

(a) First component of $\mathbf{u}$ (b) Second component of $\mathbf{u}$ (c) Profile of p

Fig. 7.3. Example 7.2: Profiles of the numerical solution.

Example 7.3. In practice, Brinkman equations are often used to model fluid flows in porous media. In this example, we choose a vuggy medium with the permeability coefficient κ highly varying. The profile of the permeability inverse is plotted in Fig. 7.2(b). Note that the exact solutions are not available for this and the next examples.

The first and the second components of the velocity obtained by SFWG method are presented in Figs. 7.4(a)-7.4(b). The pressure profile is shown in Fig. 7.4(c). The results are similar to those obtained by other methods for solving this example.

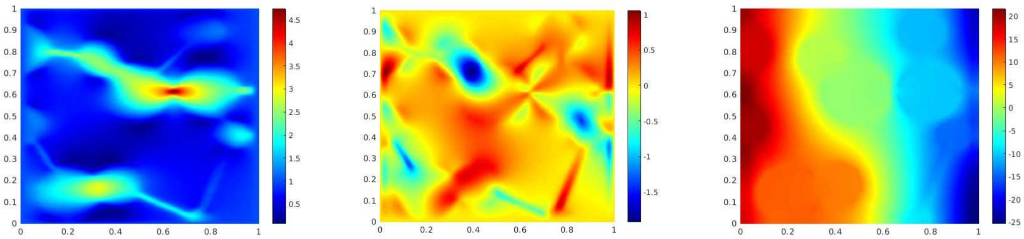

(a) First component of $\mathbf{u}$ (b) Second component of $\mathbf{u}$ (c) Profile of p

Fig. 7.4. Example 7.3: Profiles of the numerical solution.

Example 7.4. The Brinkman equations can also be used to model fluid flows in fibrous materials. A common permeability reverse for fibrous materials is shown in Fig. 7.2(c). The other input data are the same as before. And the results are plotted in Figs. 7.5(a)-7.5(c).

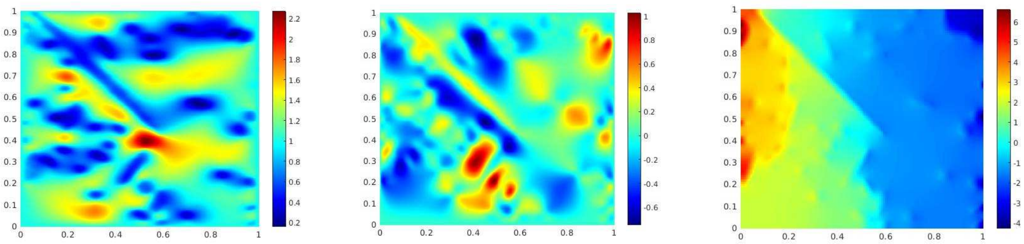

(a) First component of $\mathbf{u}$ (b) Second component of $\mathbf{u}$ (c) Profile of p

Fig. 7.5. Example 7.4: Profiles of the numerical solution.

Appendix A. Some Inequality Estimates

In this Appendix, we provide some technical results used in the paper.

Lemma A.1 ([30]). *Let $\mathcal{T}_h$ be a shape regular partition of Ω, $\mathbf{v} \in [H^{k+1}(\Omega)]^d$ and $q \in H^k(\Omega)$. Then for $0 \le s \le 1$, we have the following projection inequalities:*

$$\sum_{T\in\mathcal{T}_h} h_T^{2s}\|\mathbf{v} - Q_0\mathbf{v}\|_{s,T}^2 \le Ch^{2(k+1)}\|\mathbf{v}\|_{k+1}^2, \tag{A.1}$$

$$\sum_{T\in\mathcal{T}_h} h_T^{2s}\|\nabla\mathbf{v} - \mathbf{Q}_h(\nabla\mathbf{v})\|_{s,T}^2 \le Ch^{2k}\|\mathbf{v}\|_{k+1}^2, \tag{A.2}$$

$$\sum_{T\in\mathcal{T}_h} h_T^{2s}\|q - \mathbb{Q}_h q\|_{s,T}^2 \le Ch^{2k}\|q\|_k^2, \tag{A.3}$$

where C is a constant independent of the size of mesh h.

Let T be a cell with e as an edge/face of T. For any function $g \in H^1(T)$, the following trace inequality has been proved to be valid in [30]:

$$\|g\|_e^2 \le C\big(h_T^{-1}\|g\|_T^2 + h_T\|\nabla g\|_T^2\big). \tag{A.4}$$

Lemma A.2 ([8]). *For any $\mathbf{w} \in [H^{k+1}(\Omega)]^d$, the following inequality holds true:*

$$\|\nabla_w(\mathbf{w} - Q_h\mathbf{w})\| \le Ch^k\|\mathbf{w}\|_{k+1}. \tag{A.5}$$

Lemma A.3. *For any $\mathbf{w} \in [H^{k+1}(\Omega)]^d$, $q \in H^k(\Omega)$ and $\mathbf{v} = \{\mathbf{v}_0, \mathbf{v}_b\} \in V_h$, we have*

$$|l_1(\mathbf{w},\mathbf{v})| \le Ch^k\|\mathbf{w}\|_{k+1}|\!|\!|\mathbf{v}|\!|\!|, \tag{A.6}$$
$$|l_2(q,\mathbf{v})| \le Ch^k\|q\|_k|\!|\!|\mathbf{v}|\!|\!|, \tag{A.7}$$
$$|l_3(\mathbf{w},\mathbf{v})| \le Ch^k\|\mathbf{w}\|_{k+1}|\!|\!|\mathbf{v}|\!|\!|, \tag{A.8}$$

where $l_1(\cdot\,,\cdot)$, $l_2(\cdot\,,\cdot)$ and $l_3(\cdot\,,\cdot)$ are defined in Lemma 5.2.

Proof. Using the trace inequality (A.4), the projection inequalities (A.2)-(A.3), and (4.4), we obtain

$$\begin{aligned}
|l_1(\mathbf{w},\mathbf{v})| &= \left|\sum_{T\in\mathcal{T}_h}\langle(\nabla\mathbf{w} - \mathbf{Q}_h\nabla\mathbf{w})\cdot\mathbf{n}, \mathbf{v}_0 - \mathbf{v}_b\rangle_{\partial T}\right| \\
&\le C\left(\sum_{T\in\mathcal{T}_h} h_T\|\nabla\mathbf{w} - \mathbf{Q}_h\nabla\mathbf{w}\|_{\partial T}^2\right)^{\frac12}\left(\sum_{T\in\mathcal{T}_h} h_T^{-1}\|\mathbf{v}_0 - \mathbf{v}_b\|_{\partial T}^2\right)^{\frac12} \\
&\le Ch^k\|\mathbf{w}\|_{k+1}\|\mathbf{v}\|_{1,h} \le Ch^k\|\mathbf{w}\|_{k+1}|\!|\!|\mathbf{v}|\!|\!|.
\end{aligned}$$

Similarly, we have

$$\begin{aligned}
|l_2(q,\mathbf{v})| &= \left|\sum_{T\in\mathcal{T}_h}\langle(q - \mathbb{Q}_h q)\mathbf{n}, \mathbf{v}_0 - \mathbf{v}_b\rangle_{\partial T}\right| \\
&\le C\left(\sum_{T\in\mathcal{T}_h} h_T\|q - \mathbb{Q}_h q\|_{\partial T}^2\right)^{\frac12}\left(\sum_{T\in\mathcal{T}_h} h_T^{-1}\|\mathbf{v}_0 - \mathbf{v}_b\|_{\partial T}^2\right)^{\frac12} \\
&\le Ch^k\|q\|_k\|\mathbf{v}\|_{1,h} \le Ch^k\|q\|_k|\!|\!|\mathbf{v}|\!|\!|.
\end{aligned}$$

By (A.5), summing over all the cells, we get

$$\begin{aligned}
|l_3(\mathbf{w},\mathbf{v})| &= \left|\sum_{T\in\mathcal{T}_h}(\nabla_w(\mathbf{w} - Q_h\mathbf{w}), \nabla_w\mathbf{v})_T\right| \\
&\le Ch^k\|\mathbf{w}\|_{k+1}\|\mathbf{v}\|_{1,h} \le Ch^k\|\mathbf{w}\|_{k+1}|\!|\!|\mathbf{v}|\!|\!|.
\end{aligned}$$

This completes the proof of the lemma. □

Acknowledgements. We sincerely thank the anonymous reviewers for their insightful comments, which have helped improve the quality of this paper.

This work was supported by the National Natural Science Foundation of China (Grant Nos. 1901015, 12271208, 11971198, 91630201, 11871245, 11771179 and 11826101), and by the Key Laboratory of Symbolic Computation and Knowledge Engineering of Ministry of Education, Jilin University.

References

[1] R.A. Adams, *Sobolev Spaces*, Academic Press, 1975.

[2] A. Al-Taweel, S. Hussain, and X. Wang, A stabilizer free weak Galerkin finite element method for parabolic equation, *J. Comput. Appl. Math.*, **392** (2021), 113373.

[3] A. Al-Taweel and X. Wang, A note on the optimal degree of the weak gradient of the stabilizer free weak Galerkin finite element method, *Appl. Numer. Math.*, **150** (2020), 444–451.

[4] A.A. Avramenko, I.V. Shevchuk, M.M. Kovetskaya, and Y.Y. Kovetska, Darcy-Brinkman-Forchheimer model for film boiling in porous media, *Transp. Porous Media*, **134** (2020), 503–536.

[5] H. Brinkman, A calculation of the viscous force exerted by a flowing fluid on a dense swarm of particles, *Flow Turbul. Combust.*, **1** (1949), 27–34.

[6] E. Burman and P. Hansbo, Stabilized Crouzeix-Raviart element for the Darcy-Stokes problem, *Numer. Methods Partial Differential Equations*, **21** (2005), 986–997.

[7] E. Cáceres, G.N. Gatica, and F.A. Sequeira, A mixed virtual element method for the Brinkman problem, *Math. Models Methods Appl. Sci.*, **27** (2017), 707–743.

[8] Y. Feng, Y. Liu, R. Wang, and S. Zhang, A stabilizer-free weak Galerkin finite element method for the Stokes equations, *Adv. Appl. Math. Mech.*, **14** (2021), 181–201.

[9] L.D.P. Ferreira, T.D.S. de Oliveira, R. Surmas, M.A.P. da Silva, and R.P. Peçanha, Brinkman equation in reactive flow: Contribution of each term in carbonate acidification simulations, *Adv. Water. Resour.*, **144** (2020), 103696.

[10] F. Golfier, D. Lasseux, and M. Quintard, Investigation of the effective permeability of vuggy or fractured porous media from a Darcy-Brinkman approach, *Comput. Geosci.*, **19** (2015), 63–78.

[11] Q. Hong, F. Wang, S. Wu, and J. Xu, A unified study of continuous and discontinuous Galerkin methods, *Sci. China Math.*, **62** (2019), 1–32.

[12] Q. Hong and J. Xu, Uniform stability and error analysis for some discontinuous Galerkin methods, *J. Comp. Math.*, **39** (2021), 283–310.

[13] X. Hu, L. Mu, and X. Ye, A weak Galerkin finite element method for the Navier-Stokes equations, *J. Comput. Appl. Math.*, **362** (2019), 614–625.

[14] J. Jia, Y. Lee, Y. Feng, Z. Wang, and Z. Zhao, Hybridized weak Galerkin finite element methods for Brinkman equations, *Electron. Res. Arch.*, **29** (2021), 2489–2516.

[15] M. Juntunen and R. Stenberg, Analysis of finite element methods for the Brinkman problem, *Calcolo*, **47** (2010), 129–147.

[16] G. Kanschat, R. Lazarov, and Y. Mao, Geometric multigrid for Darcy and Brinkman models of flows in highly heterogeneous porous media: A numerical study, *J. Comput. Appl. Math.*, **310** (2017), 174–185.

[17] N. Kumar and B. Deka, Developing stabilizer free weak Galerkin finite element method for second-order wave equation, *J. Comput. Appl. Math.*, **415** (2022), 114457.

[18] H. Leng and H. Chen, Adaptive HDG methods for the Brinkman equations with application to optimal control, *J. Sci. Comput.*, **87** (2021), 46.

[19] G. Li and K. Shi, Upscaled HDG methods for Brinkman equations with high-contrast heterogeneous coefficient, *J. Sci. Comput.*, **77** (2018), 1780–1800.

[20] I. Ligaarden, M. Krotkiewski, K.A. Lie, M. Pal, and D.W. Schmid, On the Stokes-Brinkman equations for modeling flow in carbonate reservoirs, *Proceedings of the ECMOR XII – 12th European Conference on the Mathematics of Oil Recovery*, 2010.

[21] X. Liu, J. Li, and Z. Chen, A weak Galerkin finite element method for the Navier-Stokes equations, *J. Comput. Appl. Math.*, **333** (2018), 442–457.

[22] K.A. Mardal, X.C. Tai, and R. Winther, A robust finite element method for Darcy-Stokes flow, *SIAM J. Numer. Anal.* **40** (2002), 1605–1631.

[23] L. Mu, J. Wang, Y. Wang, and X. Ye, A weak Galerkin mixed finite element method for biharmonic equations, in: *Numerical Solution of Partial Differential Equations: Theory, Algorithms, and their*

Applications, **45** (2013), 247–277.
[24] L. Mu, J. Wang, and X. Ye, A stable numerical algorithm for the Brinkman equations by weak Galerkin finite element methods, *J. Comput. Phys.*, **273** (2014), 327–342.
[25] L. Mu, J. Wang, and X. Ye, Weak Galerkin finite element methods for the biharmonic equation on polytopal meshes, *Numer. Methods Partial Differ. Equ.*, **30** (2014), 1003–1029.
[26] L. Mu, J. Wang, and X. Ye, A new weak Galerkin finite element method for the Helmholtz equation, *IMA J. Numer. Anal.*, **35** (2015), 1228–1255.
[27] L. Mu, J. Wang, X. Ye, and S. Zhang, A weak Galerkin finite element method for the Maxwell equations, *J. Sci. Comput.*, **65** (2015), 363–386.
[28] Y. Qian, S. Wu, and F. Wang, A mixed discontinuous Galerkin method with symmetric stress for Brinkman problem based on the velocity-pseudostress formulation, *Comput. Methods Appl. Mech. Engrg.*, **368** (2020), 113177.
[29] J. Wang and X. Ye, A weak Galerkin finite element method for second-order elliptic problems, *J. Comput. Appl. Math.*, **241** (2013), 103–115.
[30] J. Wang and X. Ye, A weak Galerkin mixed finite element method for second order elliptic problems, *Math. Comp.*, **83** (2014), 2101–2126.
[31] J. Wang and X. Ye, A weak Galerkin finite element method for the Stokes equations, *Adv. Comput. Math.*, **42** (2016), 155–174.
[32] R. Wang, X. Wang, Q. Zhai, and R. Zhang, A weak Galerkin finite element scheme for solving the stationary Stokes equations, *J. Comput. Appl. Math.*, **302** (2016), 171–185.
[33] X. Ye and S. Zhang, A conforming discontinuous Galerkin finite element method: Part II, *Int. J. Numer. Anal. Model.*, **17** (2020), 281–296.
[34] X. Ye and S. Zhang, A stabilizer free weak Galerkin method for the biharmonic equation on polytopal meshes, *SIAM J. Numer. Anal.*, **58** (2020), 2572–2588.
[35] X. Ye and S. Zhang, A stabilizer free weak Galerkin finite element method on polytopal mesh: Part II, *J. Comput. Appl. Math.*, **394** (2021), 113525.
[36] Q. Zhai, R. Zhang, and L. Mu, A new weak Galerkin finite element scheme for the Brinkman model, *Commun. Comput. Phys.*, **19** (2016), 1409–1434.
[37] P. Zhu and S. Xie, Supercloseness and postprocessing of stabilizer-free weak Galerkin finite element approximations for parabolic problems, *Comput. Math. Appl.*, **119** (2022), 79–88.